Constraining Southern Ocean CO$_2$ Flux Uncertainty Using Uncrewed Surface Vehicle Observations

A. J. Sutton[1], N. L. Williams[2], and B. Tilbrook[3,4]

[1]Pacific Marine Environmental Laboratory, National Oceanic and Atmospheric Administration, Seattle, Washington, USA.

[2]University of South Florida, St. Petersburg, Florida, USA.

[3]Oceans and Atmosphere, Commonwealth Scientific and Industrial Research Organisation, Hobart, Tasmania, Australia.

[4]Australian Antarctic Program Partnership, University of Tasmania, Hobart, Australia.

Corresponding author: Adrienne Sutton (adrienne.sutton@noaa.gov)

Key Points:

- The first autonomous circumnavigation of Antarctica allowed for direct measurements of air-sea CO$_2$ and wind speed in the Southern Ocean.

- Bias and error propagation of various approaches to calculating CO$_2$ flux could explain some of the discrepancies between previous estimates.

- Interannual variability that is poorly-constrained by observations are also likely contributing to the discrepancies in CO$_2$ flux estimates.

Abstract

Remote, harsh conditions of the Southern Ocean challenge our ability to observe the region's influence on the climate system. Southern Ocean air-sea CO_2 flux estimates have significant uncertainty due to the reliance on limited ship-dependent observations in combination with satellite-based and interpolated data products. We utilize a new approach, making direct measurements of air-sea CO_2, wind speed, and surface ocean properties on an Uncrewed Surface Vehicle (USV). In 2019 the USV completed the first autonomous circumnavigation of Antarctica providing hourly CO_2 flux estimates. Using this unique data set to constrain potential error in different measurements and propagate those through the CO_2 flux calculation, we find that different wind speed products and sampling frequencies have the largest impact on CO_2 flux estimates with biases that range from -4% to +20%. These biases and poorly-constrained interannual variability could account for discrepancies between different approaches to estimating Southern Ocean CO_2 uptake.

Plain Language Summary

The Southern Ocean is an important part of the global climate, playing an outsized role in the uptake of heat and carbon. Yet observing the Southern Ocean is challenging due to its size, remoteness, and harsh conditions. In 2019 we completed the first autonomous circumnavigation of Antarctica with an Uncrewed Surface Vehicle (USV), also known as an ocean robot, in order to address some of these observing challenges. By directly measuring air and surface seawater carbon dioxide (CO_2) and wind speed on the USV, we were able to observe CO_2 exchange between the ocean and atmosphere every hour during the mission. Using this data set, we estimated potential errors in these measurements as well as other approaches to estimating CO_2 exchange. The use of different satellite-based wind products and sampling frequency play the largest role in uncertainty of the uptake of CO_2 in the Southern Ocean. In order to reduce this uncertainty and provide a better understanding of the Southern Ocean, expansion of an observing network made up of ships, USVs, and other autonomous devices is necessary.

1 Introduction

Covering only 30% of the global ocean surface, the Southern Ocean (most often defined as south of 30–35°S) plays an outsized role in the climate system. It is the meeting point of ocean currents and a connector between the atmosphere and ocean interior for the transfer of heat and carbon, accounting for as much as 75% and 40% of global ocean heat and carbon uptake, respectively (Frölicher et al., 2014; Khatiwala et al., 2009). While questions remain as to all of the mechanisms that contribute to CO_2 flux and the overturning circulation in the Southern Ocean, it is becoming clear that control of net CO_2 uptake over annual to decadal scales is dominated by wind-driven physical mixing and upwelling of carbon-rich deep water (Iudicone et al., 2011; Lovenduski et al., 2008).

Southern Ocean CO_2 flux is primarily a balance between the outgassing of natural carbon in upwelled waters not taken up by biological processes and the flux of anthropogenic carbon into the ocean driven by increasing atmospheric CO_2. These processes occur continuously and simultaneously as cold, carbon-rich water outgasses in upwelling regimes, and absorbs anthropogenic heat and carbon as the water flows north in the surface layer to warmer regimes. These processes vary across the diversity of Southern Ocean regimes from the temperature-

62 dominated system in the Subtropical Zone to the sea ice- and biologically-dominated regime
63 closest to Antarctica.

64   The combination of these diverse and variable biogeochemical regimes, sparse
65 observations, and inadequate constraint of circulation in models challenge estimates of Southern
66 Ocean CO_2 uptake. Climatological mean uptake estimates based on observations from ships
67 range from -0.8 to -1.0 Pg C yr^{-1} (Landschützer et al., 2014; Takahashi et al., 2009). While the
68 magnitude of interannual variability is unknown, the temporal variability of CO_2 flux at
69 interannual to decadal time scales is correlated with atmospheric variability as defined by the
70 Southern Annular Mode (SAM) index: the difference in mean sea level pressure between 40°S
71 and 65°S (Marshall, 2003). When the SAM index is positive, winds south of 45°S increase,
72 potentially accelerating upwelling of carbon-rich deep water and reducing net CO_2 uptake. A
73 negative SAM index is associated with a reduction of both upwelling and ventilation of CO_2 to
74 the atmosphere, allowing increased net CO_2 uptake. However, there are regional variations in
75 CO_2 flux response to SAM conditions that are not fully understood (Keppler and Landschützer,
76 2019; Nevison et al., 2020). Keppler and Landschützer (2019), for example, found increased
77 upwelling and CO_2 outgassing in higher latitudes during positive SAM conditions but opposing
78 effects in other regions. Several data- (Fay et al., 2014; Landschützer et al., 2015; Takahashi et
79 al., 2012) and modeling-based (Le Quéré et al., 2007; Lovenduski et al., 2007, 2008, 2015)
80 studies suggest decadal-scale variability of Southern Ocean CO_2 uptake is within ±0.4 Pg C yr^{-1},
81 a significant portion of the climatological mean estimate of -0.8 to -1.0 Pg C yr^{-1}.

82   New observations, however, challenge whether the Southern Ocean is a strong sink.
83 Biogeochemical float data from 2014–2017 estimate a Southern Ocean CO_2 flux of -0.08 Pg C
84 yr^{-1} (Gray et al., 2018), an order of magnitude less than the climatological mean estimates based
85 on ship-based surface ocean CO_2 partial pressure (pCO_2) data products (Landschützer et al.,
86 2016, 2014; Rödenbeck et al., 2015; Takahashi et al., 2009). Even after correcting for a potential
87 bias of 4 µatm to the float-based calculated seawater pCO_2, discrepancies between ship- and
88 float-based CO_2 flux estimates remain (Bushinsky et al., 2019). Whether recent float-based CO_2
89 flux estimates represent an updated understanding of the climatological mean, float-based
90 seawater pCO_2 requires an even larger bias correction, or 2014–2017 conditions were
91 anomalous, is currently unresolved.

92   A criticism of ship-based estimates is the scarcity of data in both time and space,
93 especially during winter months. However, surface ocean pCO_2 is measured directly on ships
94 with low uncertainty (±0.5%) (Pierrot et al., 2009), compared to pCO_2 calculated from float pH
95 measurements and estimated total alkalinity that has a higher uncertainty (±2.8%) (Bushinsky et
96 al., 2019; Williams et al., 2017). Unlike ships, floats are able to sample in harsh winter
97 conditions unfit for safe ship operations as well as under ice, increasing the potential for filling
98 observational gaps. Another issue impacting the uncertainty in both float- and ship-based
99 climatological CO_2 flux estimates is the use of observation-derived atmospheric CO_2 products
100 and satellite-based wind and sea level pressure products, which have been shown to add
101 significant uncertainty to CO_2 flux estimates in some regions (Chiodi et al., 2019; Roobaert et
102 al., 2018; Sutton et al., 2017).

103   Technological advances of Uncrewed Surface Vehicles (USVs) address these
104 observational challenges through remote surveying in harsh conditions with direct measurements
105 of air-sea pCO_2 and wind speed. Here we present results from the first autonomous
106 circumnavigation of Antarctica, a 22,000-km, 196-day mission. A Saildrone Inc. USV with an

107   integrated Autonomous Surface Vehicle CO_2 (ASVCO$_2$™) system was designed specifically to
108   survive the forces of being rolled and submerged by 15-meter breaking waves in the Southern
109   Ocean. We calculate air-sea CO_2 flux from the USV and provide a thorough comparison of
110   potential bias in CO_2 flux calculated with direct measurements relative to recent float-based
111   methods (Bushinsky et al., 2019; Gray et al., 2018) and a ship-based data product (Landschützer
112   et al., 2020) that rely on other satellite- and observational-based data products. We then discuss
113   the potential role of flux uncertainty and interannual variability in determining the Southern
114   Ocean carbon sink.

115   **2 Materials and Methods**

116   2.1 USV and sensors

117   The Saildrone USV is an ocean-going drone navigable via satellite communications with
118   wind-driven propulsion and primarily solar-powered meteorological and surface ocean physical,
119   chemical, and biological sensors. The Saildrone USV that completed the 2019 Antarctica
120   circumnavigation is similar to the standard vehicles with a 7 m hull and 2.5 m keel described by
121   Meinig et al. (2019) and Zhang et al. (2019) but includes an adapted wing to survive the extreme,
122   high winds and waves of the Southern Ocean (Figure 1). This USV design includes a lower-
123   aspect square rig designed to withstand the force of being rolled and submerged by 15 m
124   breaking waves but limits navigation to sailing primarily downwind. This design has been
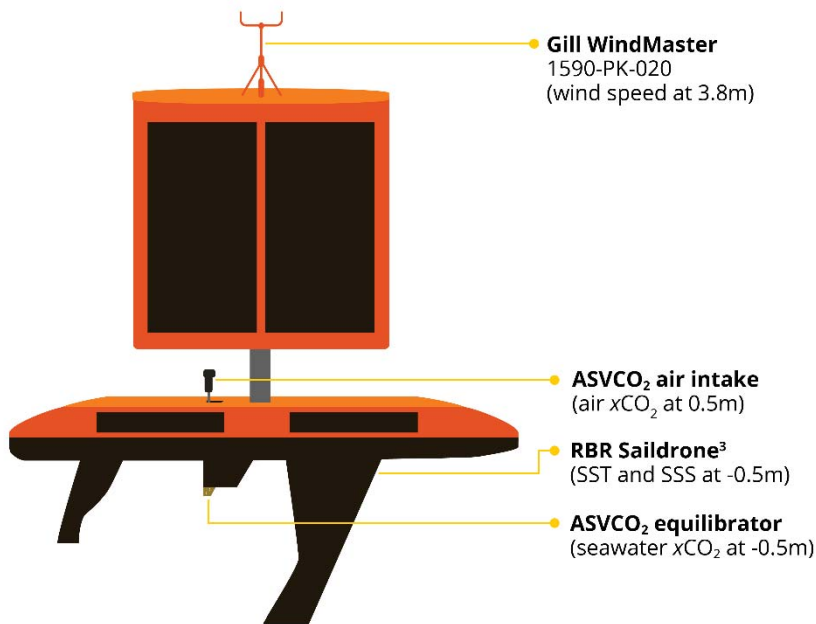125   recently modified to improve maneuverability.

126   Meteorological sensors are mounted on the square wing, including a Gill WindMaster™
127   anemometer at 3.8 m height. Through field intercomparisons, Zhang et al. (2019) found RMS
128   differences of $\pm$0.6–1.0 m s^{-1} between wind speed measured on Saildrone USVs with the
129   standard 5 m wing compared to both the Woods Hole Oceanographic Institute's buoy Air-Sea
130   Interaction METeorology System and the R/V *Revelle*. In this study, we use the higher-bound
131   wind speed error of $\pm$1.0 m s^{-1} derived by Zhang et al. (2019) for the estimated error of wind
132   speed measured from the shorter wing at 3.8 m. Even though they determined that bias was
133   inconclusive, to generate conservative estimates we use the mean bias determined from Zhang et
134   al. (2019) intercomparisons of +0.2 m s^{-1}.

135   The ASVCO$_2$™ system is packaged in a waterproof enclosure mounted in the USV hull.
136   The ASVCO$_2$ is nearly identical to the Moored Autonomous pCO$_2$ (MAPCO$_2$™) system that has
137   been used for over two decades on dozens of surface buoys and has a lab- and field-validated
138   uncertainty of $\pm$2 μatm or $\pm$0.5% (Sabine et al., 2020; Sutton et al., 2014). These CO_2 systems
139   utilize an equilibrator-based gas collection system and an infrared gas analyzer (LI-820, LI-
140   COR™) calibrated in situ with reference gas traceable to World Meteorological Organization
141   standards, a similar methodology to the underway pCO$_2$ system deployed on the global network
142   of ships of opportunity (Pierrot et al., 2009). In order to adapt the MAPCO$_2$ for USV
143   deployments, the ASVCO$_2$ includes an equilibrator mounted to the USV hull with a fairing
144   added to maintain consistent water level in the equilibrator when moving at speeds greater than 4
145   knots (Figure 1).

146   The ASVCO$_2$ system collects 1-hourly measurements of sea surface and marine
147   boundary layer atmospheric xCO$_2$ (the mole fraction of CO_2) and sea level atmospheric pressure.
148   Each xCO$_2$ measurement is paired with sea surface temperature (SST) and salinity (SSS)
149   collected by an RBR Saildrone[3] CTD customized for mounting through the Saildrone USV keel

150   at 0.5 m depth. Seawater and air pCO_2 (at in situ SST) is calculated according to standard
151   operating procedures (Dickson et al., 2007; Weiss, 1974) as described in Sutton et al. (2014).
152   Data from the $ASVCO_2$ system and wind speed, SST, and SSS are archived at the National
153   Centers for Environmental Information (Sutton et al., 2020).

154   The USV was deployed from Bluff, New Zealand on 19 January 2019. Sailing
155   downwind, the USV navigated east 22,000 km around Antarctica and was recovered off Bluff on
156   3 August 2019, 196 days later. The anemometer was damaged near the Drake Passage during an
157   iceberg collision at the end of March.
158

Gill WindMaster
1590-PK-020
(wind speed at 3.8m)

$ASVCO_2$ air intake
(air xCO_2 at 0.5m)

RBR Saildrone[3]
(SST and SSS at -0.5m)

$ASVCO_2$ equilibrator
(seawater xCO_2 at -0.5m)

159

160   **Figure 1**. Schematic diagram of the 2019 Southern Ocean Saildrone USV and location of the
161   sensors used in this study. Schematic is not to scale.

162   2.2 Comparison data sets

163   Several data sets are used as comparisons for the USV-derived CO_2 fluxes. The first is
164   v2020 of the SOM-FFN neural network product documented in Landschützer et al. (2016),
165   which uses ship-based measurements of seawater pCO_2 to estimate monthly air-sea CO_2 fluxes
166   globally over the period 1982 to 2019 (Landschützer et al., 2020). The second product is the
167   same SOM-FFN neural network, but with the addition of Southern Ocean Carbon and Climate
168   Observations and Modeling project (SOCCOM) float-derived pCO_2 as training datasets
169   (Bushinsky et al., 2019). This product is available as "SOCCOM-only" as well as
170   "SOCCOM+ship" for the years 2014 to 2017. To compare these two data sets with the USV, we
171   subsample each product at the location and month of each USV CO_2 flux measurement and
172   average the CO_2 fluxes over 10-day periods.
173   The third comparison dataset is air-sea CO_2 fluxes estimated from calculated surface
174   ocean pCO_2 from SOCCOM biogeochemical float data from 2015 to 2019, which is available

175 online as a quality-controlled data snapshot dated 30 August 2020 (Johnson et al., 2020). All
176 float profiles from 2015 to 2019 were separated by year and front locations, and subsequently
177 averaged by month to create monthly pCO_2 and CO_2 flux estimates for each of the three major
178 zones discussed in this manuscript. The Subantarctic Zone is defined as profiles with an oxygen
179 minimum deeper than 1200 m, a salinity maximum deeper than 500 m, and surface waters
180 fresher than 34.6. The Polar Frontal zone is defined as profiles with an oxygen minimum
181 between 900 and 1200 m deep and a deep (>1400 m) salinity maximum. The Antarctic Zone is
182 defined as profiles with an oxygen minimum between 600 and 900 m deep and a salinity
183 maximum deeper than 1000 m. While there are some profiles within the Seasonal Sea Ice Zone
184 which fall within the definitions above, these profiles are not included in the analysis if they
185 occur during a calendar year when that float profiled under ice. In contrast to previous studies,
186 the float profiles have not been extrapolated over time and the monthly averages only represent
187 averages of the instantaneous fluxes at the time of the float surfacing.

188 We use CO_2 flux provided by the first two comparison data sets (Bushinsky et al., 2019
189 and Landschützer et al., 2020). CO_2 flux for the third comparison data set (SOCCOM
190 biogeochemical floats from 2015 to 2019) and the USV are calculated using established
191 methodologies summarized in the Supplemental.
192

3 Results and discussion

3.1 Air-sea observations

195 During the mission, the USV observed a large range in ΔpCO_2 (seawater – air pCO_2) of
196 33 to -40 µatm with a slightly negative mean of -4 µatm and a variance of $\pm$ 12 µatm (Figure 2).
197 Although periods of negative and positive ΔpCO_2 were observed throughout the deployment,
198 positive ΔpCO_2 indicating outgassing was prevalent during the latter part of the deployment,
199 primarily during late fall and early winter in the Indian Ocean sector of the Antarctic Zone
200 (Figure S1). Observed mean, variation, and range of air xCO_2, sea pCO_2, ΔpCO_2, SST, SSS, and
201 wind speed are given in Table S2.

3.2 CO_2 flux uncertainty analysis

203 The uncertainty in calculated CO_2 flux can vary widely given the different options of
204 inputs. The gas transfer velocity (k) uncertainty of 20% applies to all CO_2 flux estimates
205 (Wanninkhof, 2014), leaving the choice and availability of wind speed, seawater pCO_2, and air
206 pCO_2 data sets the major sources of variation among different approaches.

207 Given the scarcity of in situ wind speed observations, the use of satellite-based wind
208 speed in calculating CO_2 flux is common. However, in many regions, these satellite-based
209 products have biases in comparison to available in situ data (Hihara et al., 2015; Kent et al.,
210 2013; Tomita et al., 2015; Wallcraft et al., 2009; Weissman et al., 2012) and can have significant
211 impacts on CO_2 flux estimates (Chiodi et al., 2019; Roobaert et al., 2018; Sutton et al., 2017).
212 Directly-measured wind speed also suffer errors due to flow distortion, platform movement, and
213 wave shadowing, resulting in uncertainties of $\pm$0.1 m s^{-1} on buoys (Cronin et al., 2008; Kubota et
214 al., 2008; Weller, 2015) and up to $\pm$1.0 m s^{-1} on Saildrone USVs (Zhang et al., 2019).

215 Prior to the USV anemometer being damaged in March 2019, there is no mean difference
216 between USV-measured and Cross-Calibrated Multi-Platform Near Real Time V2.0 (CCMP V2)

217   wind speed (Mears et al., 2019) or ERA-Interim Reanalysis (Dee et al., 2011) wind speed with a
218   variance around wind speed residuals of ±1.8 m s^{-1} and ±2.0 m s^{-1}, respectively (Figure S2).
219   NCEP-DOE AMIP-II Reanalysis 2 (NCEP-2) (Kanamitsu et al., 2002) and ERA5 (Hersbach et
220   al., 2020) wind speeds have lower wind speed by 1.0 and 0.1 m s^{-1}, respectively, than measured
221   on the USV with a variance around the mean bias of ±3.9 and ±1.4 m s^{-1}, respectively. In Table
222   S1 these biases are reported relative to the "true" wind speed by correcting for the USV wind
223   speed bias of $+0.2$ m s^{-1} (Zhang et al., 2019). Importantly, the biases in satellite-based wind
224   speed products relative to the USV-measured wind speed are not randomly distributed. Satellite
225   and USV wind speeds tend to agree most closely at wind speeds of 10 m s^{-1}, but diverge at lower
226   and higher wind speeds (Figure S2c). These results are consistent with biases reported in other
227   intercomparisons mentioned previously and summarized by Cronin et al. (2019).

228   Uncertainties associated with ship-, USV-, and float-based sources of pCO$_2$ are ±0.5%,
229   ±0.5%, and ±2.8%, respectively (Table S1.) Common data sources of atmospheric baseline xCO$_2$
230   are the NOAA Greenhouse Gas Marine Boundary Layer (MBL) Reference CO$_2$ product
231   (Dlugokencky et al., 2019) or observations from nearby atmospheric observatories, like at Cape
232   Grim. Monthly mean xCO$_2$ from these two sources and the USV tend to agree within 0.2 ppm;
233   however, shorter-term variability indicating terrestrial biosphere influence is prevalent within the
234   hourly USV observations (Figure S3) and the hourly in situ Cape Grim observations (data not
235   shown). Converting these sources of xCO$_2$ to pCO$_2$ requires atmospheric pressure at sea level,
236   which if using satellite-based products such as NCEP 2, ERA-Interim, or ERA5 introduces
237   another possible source of error (Table S1).

238   Various sampling frequencies of these data sources can also introduce error into the CO$_2$
239   flux calculation. Monthly CO$_2$ flux calculated from subsampling the hourly USV ΔpCO$_2$ data set
240   at 6-hourly intervals, which is the common temporal frequency of satellite-based products,
241   results in nearly identical values to monthly flux calculated from the hourly observations (Figure
242   S4). However, subsampling the hourly data set at all possible 10-day sampling frequencies, the
243   timescale for float observations, results in an integrated bias in CO$_2$ flux of $+0.05$ g C m^{-2} mo^{-1} or
244    $+23$% (less uptake/more outgassing) over the 7-month comparison period with large variation
245   around the monthly means due to the high temporal variability of the data set at a scale of less
246   than 10 days.

247   Propagated bias of USV-derived CO$_2$ flux is -4% (less outgassing/more uptake) driven by
248   the potential bias in USV-measured wind speed (Table 1). In this case, USV, CCMP V2, and
249   ERA-Interim wind speed bias are equivalent and have the same impact on calculated CO$_2$ flux.
250   Replacing directly-measured air pCO$_2$ with pCO$_2$ calculated from MBL or Cape Grim values and
251   NCEP 2, ERA-Interim, or ERA5 sea level pressure does not significantly impact flux bias.
252   Taking into consideration the potential bias of subsampling at 10-day intervals combined with
253   the ERA-Interim wind speed bias results in an overall positive bias of $+20$% (more
254   outgassing/less uptake) in calculated CO$_2$ flux primarily due to the bias in subsampling the 2019
255   USV data set at 10-day intervals. Monteiro et al. (2015) found that a 10-day sampling period in
256   spring-summer in the Subantarctic Zone resulted in a 10-25% increase in uncertainty in CO$_2$ flux
257   relative to hourly sampling due to mixed layer responses to storm events, which may explain a
258   similar magnitude sampling bias observed with the USV results.

259

260 **Table 1**. Estimated bias for different approaches of calculating CO_2 flux by applying mean bias
261 from Table S1 to conditions observed during the 2019 USV deployment. Resulting biases are
262 additive based on mean biases reported in Table S1. A negative bias suggests less
263 outgassing/more uptake; positive suggests more outgassing/less uptake. The USV CO_2 flux bias
264 results from the estimated USV wind speed bias of $+0.2$ m s^{-1} (Zhang et al., 2019).

265

Seawater pCO_2 data source	Air pCO_2 data source	Wind speed data source	Estimated CO_2 flux bias
USV	USV	USV	-4%
Ship or USV	Ship, USV, MBL, or Gape Grim	CCMP-NRT or ERA-Interim	-4%
Float-derived	MBL or Cape Grim	ERA-Interim	+20%

266

267 3.3 CO_2 flux comparisons

268   Due to the loss of the wind speed sensor during the USV deployment, USV CO_2 flux
269 presented in this section is calculated using CCMP V2 wind speed. During the 2019
270 circumnavigation, the USV observed periods of strong outgassing as high as 10.5 g C m^{-2} mo^{-1} in
271 June and July in the Antarctic Zone, which was one of the zones where SOCCOM float-based
272 data from 2014–2017 showed stronger outgassing than the SOM-FFN ship-based climatology
273 (Figure 3a; Bushinsky et al., 2019; Gray et al., 2018). There were also periods of intense short-
274 scale CO_2 uptake during February through April, some of which were associated with
275 phytoplankton blooms (data not shown). The periods of strong outgassing observed by the USV
276 in June and July overlap with the Bushinsky et al. (2019) 2014–2017 SOCCOM-only SOM-FFN
277 estimates of CO_2 outgassing (Figure 3a). However, the USV observations show these outgassing
278 events occur over time periods from hours to two days in length, and these short-lived outgassing
279 events do not lead to outgassing as strong as the SOCCOM-only SOM-FFN estimates when
280 averaged at the 10-day scale. Mean USV CO_2 flux in June and July results in a weak net
281 outgassing of 0.7 g C m^{-2} mo^{-1}, more similar to the Landschützer et al. (2020) ship-based data
282 product and the Bushinsky et al. (2019) combined SOCCOM-ship SOM-FFN product than the
283 SOCCOM-only SOM-FFN product.
284

285
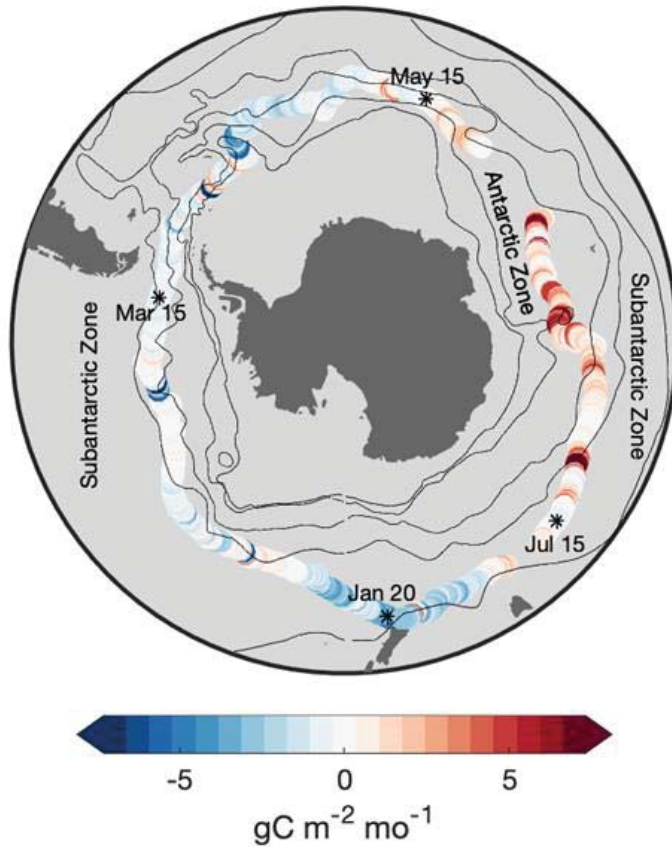
Figure 2. CO$_2$ flux calculated from USV-measured ΔpCO$_2$, SST, and SSS and CCMP-NRT
wind speed. Dates and * show the location of the USV with time. Black lines indicate
climatological locations of the major fronts from Orsi et al. (1995) as in Figure S1.

Focusing only on 2019 observations, USV-measured and float-estimated surface seawater
pCO$_2$ are consistent within standard deviations of monthly means within the Subantarctic Zone
and the Antarctic Zone, the two major zones sampled by the 2019 Saildrone USV (Figure S5).
Within the Antarctic Zone where Gray et al. (2018) found the largest winter-time discrepancy
between float- and ship-based data, we find a mean difference of 0.5 ± 2.6 g C m^{-2} mo^{-1} (or no
significant difference) between USV and float-derived CO$_2$ flux in March through July 2019
(Figure 3b). To test the possible effect of variable float locations on the estimates of CO$_2$ flux in
the Antarctic Zone, the Landschützer v2020 SOM-FFN ship-based climatology was subsampled
at the times and locations of each float observation. Float-based fluxes are on average 1.5 g C m^{-2} mo^{-1} greater than the ship-based climatology in this zone for 2015–2019 with significant
interannual variability (2015: +3.9, 2016: +2.1, 2017: +0.6, 2018: +0.8, and 2019: -0.1 g C m^{-2} mo^{-1}).

Figure 3b illustrates this significant interannual variability in float-derived CO$_2$ flux in
the Antarctic Zone from 2015–2019. Net CO$_2$ uptake observed by the USV and floats in 2019
contrasts with the strong outgassing during winter of 2015 and 2016. This interannual variability
may be influenced by SAM with increased westerly wind strength during the more positive
phases of SAM increasing upwelling of relatively CO$_2$-rich waters. The greatest outgassing is

307 observed in the Antarctic Zone during strong positive phases of SAM in 2015 and 2016 (Figures
308 3b and S6). The USV data were collected during a decline in the SAM index and are similar to
309 the float-based net flux estimates for 2019 (Figure 3b).
310

311
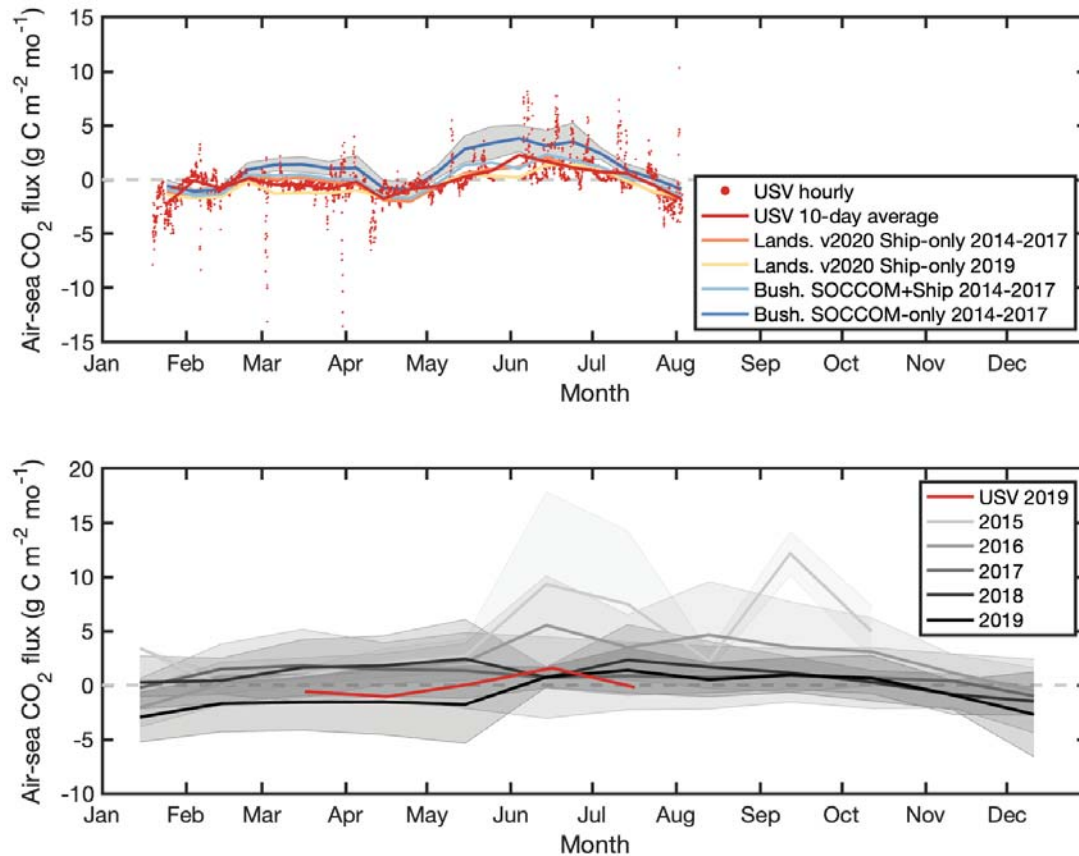
312 **Figure 3**. a) Time series of monthly CO_2 flux calculated using all USV observations at hourly
313 (red dots) and 10-day averaged (red line) time steps; from Landschützer et al. (2020) SOM-FFN
314 ship-based climatology (orange) and 2019 (yellow) subsampled at the Saildrone locations and
315 times and averaged over 10 days; and from Bushinsky et al. (2019) using the same methods of
316 the SOM-FFN v2020 ship-based climatology for the years 2014–2017 but incorporating
317 seawater pCO_2 estimated from both ships and SOCCOM biogeochemical-float observations
318 (light blue), and using only SOCCOM biogeochemical float observations (dark blue) for the
319 years 2014–2017. The shaded area represents the interannual variability in the SOCCOM-only
320 product over 2014–2017. b) Antarctic Zone monthly-averaged USV fluxes (red) plotted with
321 monthly mean SOCCOM float-based CO_2 flux from 2015–2019 in that zone (gray). The shaded
322 area is 1 σ of monthly mean SOCCOM CO_2 flux.
323

324   Analysis of the Saildrone USV observations reveal several potential sources of bias and
325 error in USV-, ship-, and float-based CO_2 flux (Tables S1 and 1). Given the significant fine-scale
326 temporal and spatial variability observed during 2019, the 10-day sampling routine of floats may
327 introduce a bias (more outgassing/less uptake in this case), which could account for some of the
328 difference between float- and ship-based CO_2 flux reported previously (Bushinsky et al., 2019;
329 Gray et al., 2018). It is also critical to better constrain how shifts in SAM conditions play a role

330 in Southern Ocean CO_2 flux. The larger differences between the ship-based climatology and
331 float-based flux during prolonged positive SAM conditions in 2015–2016 suggests an influence
332 of measurement bias during those years or the possibility that the ship-based climatology does
333 not constrain increased upwelling of CO_2-rich water in higher latitudes. Sustained observations
334 are needed to better constrain interannual variability like the anomalous strong winter outgassing
335 observed by floats in 2015–2016 relative to 2017–2019. Better coverage of ships, USVs, and
336 floats are needed to resolve these uncertainties in measurements and variability in the Southern
337 Ocean.

4 Conclusions

339   Climate change is predicted to reduce ocean CO_2 uptake under climate model scenarios
340 that show intensification of winds and acceleration of the overturning circulation in the Southern
341 Ocean (Le Quéré et al., 2007). Over the next century models also predict reductions in sea-ice
342 cover and surface ocean warming, freshening, and stratification, which are all expected to impact
343 the carbon sink. How these processes impact the overall balance of CO_2 outgassing and uptake in
344 the Southern Ocean is uncertain. Better representation of these processes in models is necessary
345 to predict the Southern Ocean's role in a future climate.

346   Our results indicate that the strong wintertime outgassing observed by floats in 2015 and
347 2016 was not prevalent in 2019. The change may be linked to a decline in the SAM index in the
348 later years leading to a reduction in upwelling of CO_2 rich waters to the surface. More sustained
349 observations are needed to constrain interannual variability and the impact on both Southern
350 Ocean and global ocean CO_2 uptake estimates. The first circumnavigation of the Southern Ocean
351 by a USV described here has shown the capability to collect high quality data that can be used to
352 constrain multi-platform measurement uncertainties and interrogate how variability from the
353 scale of hours to years may impact CO_2 flux estimates.

354   A multi-platform observing network consisting of USVs directly surveying air-sea
355 interactions, floats measuring full water column biogeochemistry even under ice, and the ship-
356 based measurements for ground-truthing autonomous sensors would, in combination, best track
357 changes in ocean carbon uptake and better constrain variability. USVs fill a unique niche with
358 the ability to survey regions for extended periods where ships do not routinely operate, opening
359 up new opportunities for filling persistent gaps in the ocean observing system with high-quality
360 pCO_2 and meteorological observations.

References

379   Bushinsky, S. M., Landschützer, P., Rödenbeck, C., Gray, A. R., Baker, D., Mazloff, M. R., et al.
380   (2019). Reassessing Southern Ocean air-sea CO_2 flux estimates with the addition of
381   biogeochemical float observations. *Global Biogeochemical Cycles, 33*(11), 1370–1388.
382   https://doi.org/10.1029/2019GB006176

383   Chiodi, A. M., Dunne, J. P., & Harrison, D. E. (2019). Estimating air-sea carbon flux uncertainty
384   over the tropical Pacific: Importance of winds and wind analysis uncertainty. *Global
385   Biogeochemical Cycles, 33*, 370–390. https://doi.org/10.1029/2018GB006047

386   Cronin, M. F., Gentemann, C. L., Edson, J., Ueki, I., Bourassa, M., Brown, S., et al. (2019). Air-
387   sea fluxes with a focus on heat and momentum. *Frontiers in Marine Science, 6*, 430.
388   https://doi.org/10.3389/fmars.2019.00430

389   Cronin, M. F., Meinig, C., Sabine, C. L., Ichikawa, H., & Tomita, H. (2008). Surface mooring
390   network in the Kuroshio Extension. *IEEE Systems Special Issue on GEOSS, 2*(3), 424–
391   430.

392   Dee, D. P., Uppala, S. M., Simmons, A. J., Berrisford, P., Poli, P., Kobayashi, S., et al. (2011).
393   The ERA-Interim reanalysis: configuration and performance of the data assimilation
394   system. *Quarterly Journal of the Royal Meteorological Society, 137*(656), 553–597.
395   https://doi.org/10.1002/qj.828

396   Dickson, A. G., Sabine, C. L., & Christian, J. R. (Eds.). (2007). *Guide to Best Practices for
397   Ocean CO_2 Measurements*: North Pacific Marine Science Organization.

398   Dlugokencky, E. G., Thoning, K. W., Lang, P. M., & Tans, P. P. (2019). NOAA Greenhouse Gas
399   Reference from Atmospheric Carbon Dioxide Dry Air Mole Fractions from the NOAA
400   ESRL Carbon Cycle Cooperative Global Air Sampling Network. Data Path:
401   ftp://aftp.cmdl.noaa.gov/data/trace_gases/co2/flask/surface/ [Accessed 1 August 2019]

402   Fay, A. R., McKinley, G. A., & Lovenduski, N. S. (2014). Southern Ocean carbon trends:
403   Sensitivity to methods. *Geophysical Research Letters, 41*(19), 6833–6840.
404   https://doi.org/10.1002/2014GL061324

405   Frölicher, T. L., Sarmiento, J. L., Paynter, D. J., Dunne, J. P., Krasting, J. P., & Winton, M.
406   (2014). Dominance of the Southern Ocean in anthropogenic carbon and heat uptake in
407   CMIP5 models. *Journal of Climate, 28*(2), 862–886. https://doi.org/10.1175/JCLI-D-14-
408   00117.1

409   Gray, A. R., Johnson, K. S., Bushinsky, S. M., Riser, S. C., Russell, J. L., Talley, L. D., et al.
410   (2018). Autonomous biogeochemical floats detect significant carbon dioxide outgassing
411   in the high-latitude Southern Ocean. *Geophysical Research Letters, 45*(17), 9049–9057.
412   https://doi.org/10.1029/2018GL078013

413 Hersbach, H., Bell, B., Berrisford, P., Hirahara, S., Horányi, A., Muñoz-Sabater, J., et al. (2020).
414   The ERA5 global reanalysis. 146(730), 1999-2049.

415 Hihara, T., Kubota, M., & Okuro, A. (2015). Evaluation of sea surface temperature and wind
416   speed observed by GCOM-W1/AMSR2 using in situ data and global products. *Remote*
417   *Sensing of Environment, 164*, 170–178. https://doi.org/10.1016/j.rse.2015.04.005

418 Iudicone, D., Rodgers, K. B., Stendardo, I., Aumont, O., Madec, G., Bopp, L., et al. (2011).
419   Water masses as a unifying framework for understanding the Southern Ocean carbon
420   cycle. *Biogeosciences, 8*(5), 1031–1052. https://doi.org/10.5194/bg-8-1031-2011

421 Johnson, K. S., Riser, S. C., Boss, E. S., Talley, L. D., Sarmiento, J. L., Swift, D. D., et al.
422   (2020). SOCCOM float data - Snapshot 2020-08-30. In Southern Ocean Carbon and
423   Climate Observations and Modeling (SOCCOM) Float Data Archive. UC San Diego
424   Library Digital Collections. https://doi.org/10.6075/J0BK19W5

425 Kanamitsu, M., Ebisuzaki, W., Woollen, J., Yang, S.-K., Hnilo, J. J., Fiorino, M., & Potter, G. L.
426   (2002). NCEP–DOE AMIP-II Reanalysis (R-2). *Bulletin of the American Meteorological*
427   *Society, 83*(11), 1631–1644. https://doi.org/10.1175/BAMS-83-11-1631

428 Kent, E. C., Fangohr, S., & Berry, D. I. (2013). A comparative assessment of monthly mean
429   wind speed products over the global ocean. *International Journal of Climatology, 33*(11),
430   2520–2541. https://doi.org/10.1002/joc.3606

431 Keppler, L., & Landschützer, P. (2019). Regional wind variability modulates the Southern Ocean
432   carbon sink. *Scientific Reports, 9*(1), 7384. https://doi.org/10.1038/s41598-019-43826-y

433 Khatiwala, S., Primeau, F., & Hall, T. (2009). Reconstruction of the history of anthropogenic
434   CO_2 concentrations in the ocean. *Nature, 462*(7271), 346–349.
435   https://doi.org/10.1038/nature08526

436 Kubota, M., Iwabe, N., Cronin, M. F., & Tomita, H. (2008). Surface heat fluxes from the
437   NCEP/NCAR and NCEP/DOE reanalyses at the KEO buoy site. *Journal of Geophysical*
438   *Research Oceans, 113*, C02009.

439 Landschützer, P., Gruber, N., & Bakker, D. C. E. (2016). Decadal variations and trends of the
440   global ocean carbon sink. *Global Biogeochemical Cycles, 30*(10), 1396–1417.
441   https://doi.org/10.1002/2015GB005359

442 Landschützer, P., Gruber, N., & Bakker, D. C. E. (2020). An observation-based global monthly
443   gridded sea surface pCO_2 product from 1982 onward and its monthly climatology (NCEI
444   Accession 0160558). Version 5.5. NOAA National Centers for Environmental
445   Information. Dataset. https://doi.org/10.7289/V5Z899N6 [Accessed 2020-07-10]

446 Landschützer, P., Gruber, N., Bakker, D. C. E., & Schuster, U. (2014). Recent variability of the
447   global ocean carbon sink. *Global Biogeochemical Cycles, 28*, 927–949.
448   https://doi.org/10.1002/2014GB004853

449 Landschützer, P., Gruber, N., Haumann, F. A., Rödenbeck, C., Bakker, D. C. E., van Heuven, S.,
450   et al. (2015). The reinvigoration of the Southern Ocean carbon sink. *Science, 349*(6253),
451   1221–1224. https://doi.org/10.1126/science.aab2620

452   Large, W. G., & Pond, S. (1981). Open ocean momentum flux measurements in moderate to
453   strong winds. *Journal of Physical Oceanography, 11*(3), 324–336.
454   https://doi.org/10.1175/1520-0485(1981)011<0324:OOMFMI>2.0.CO;2

455   Le Quéré, C., Rödenbeck, C., Buitenhuis, E. T., Conway, T. J., Langenfelds, R., Gomez, A., et
456   al. (2007). Saturation of the Southern Ocean CO_2 sink due to recent climate change.
457   *Science, 316*(5832), 1735–1738. https://doi.org/10.1126/science.1136188

458   Lovenduski, N. S., Fay, A. R., & McKinley, G. A. (2015). Observing multidecadal trends in
459   Southern Ocean CO_2 uptake: What can we learn from an ocean model? *Global
460   Biogeochemical Cycles, 29*(4), 416–426. https://doi.org/10.1002/2014GB004933

461   Lovenduski, N. S., Gruber, N., & Doney, S. C. (2008). Toward a mechanistic understanding of
462   the decadal trends in the Southern Ocean carbon sink. *Global Biogeochemical Cycles,
463   22*(3), GB3016. https://doi.org/10.1029/2007GB003139

464   Lovenduski, N. S., Gruber, N., Doney, S. C., & Lima, I. D. (2007). Enhanced CO_2 outgassing in
465   the Southern Ocean from a positive phase of the Southern Annular Mode. *Global
466   Biogeochemical Cycles, 21*(2), GB2026. https://doi.org/10.1029/2006GB002900

467   Marshall, G. J. (2003). Trends in the Southern Annular Mode from observations and reanalyses.
468   *Journal of Climate, 16*(24), 4134–4143. https://doi.org/10.1175/1520-
469   0442%282003%29016%3C4134%3ATITSAM%3E2.0.CO%3B2

470   Mears, C. A., Scott, J., Wentz, F. J., Ricciardulli, L., Leidner, S. M., Hoffman, R., & Atlas, R.
471   (2019). A near-real-time version of the Cross-Calibrated Multiplatform (CCMP) ocean
472   surface wind velocity data set. *Journal of Geophysical Research Oceans, 124*(10), 6997–
473   7010. https://doi.org/10.1029/2019JC015367

474   Meinig, C., Burger, E. F., Cohen, N., Cokelet, E. D., Cronin, M. F., Cross, J. N., et al. (2019).
475   Public–private partnerships to advance regional ocean-observing capabilities: A
476   Saildrone and NOAA-PMEL case study and future considerations to expand to global
477   scale observing. *Frontiers in Marine Science, 6,* 448.
478   https://doi.org/10.3389/fmars.2019.00448

479   Monteiro, P. M. S., Gregor, L., Lévy, M., Maenner, S., Sabine, C. L., & Swart, S. (2015).
480   Intraseasonal variability linked to sampling alias in air-sea CO_2 fluxes in the Southern
481   Ocean. *Geophysical Research Letters, 42*(20), 8507–8514.
482   https://doi.org/10.1002/2015GL066009

483   Nevison, C. D., Munro, D. R., Lovenduski, N. S., Keeling, R. F., Manizza, M., Morgan, E. J., &
484   Rödenbeck, C. (2020). Southern Annular Mode influence on wintertime ventilation of the
485   Southern Ocean detected in atmospheric O2 and CO2 measurements. *Geophysical
486   Research Letters, 47,* e2019GL085667. https://doi.org/10.1029/2019GL085667

487   Orsi, A. H., Whitworth, T., & Nowlin, W. D. (1995). On the meridional extent and fronts of the
488   Antarctic Circumpolar Current. *Deep Sea Research Part I: Oceanographic Research
489   Papers, 42*(5), 641–673. https://doi.org/10.1016/0967-0637(95)00021-W

490   Pierrot, D., Neill, C., Sullivan, K., Castle, R., Wanninkhof, R., Lüger, H., et al. (2009).
491   Recommendations for autonomous underway $p$$CO_2$ measuring systems and data-
492   reduction routines. *Deep Sea Research Part II: Topical Studies in Oceanography, 56*(8–
493   10), 512–522. https://doi.org/10.1016/j.dsr2.2008.12.005

494 Rödenbeck, C., Bakker, D. C. E., Gruber, N., Iida, Y., Jacobson, A. R., Jones, S., et al. (2015).
495 Data-based estimates of the ocean carbon sink variability – first results of the Surface
496 Ocean pCO2 Mapping intercomparison (SOCOM). *Biogeosciences*, 12(23), 7251-7278.

497 Roobaert, A., Laruelle, G. G., Landschützer, P., & Regnier, P. (2018). Uncertainty in the global
498 oceanic CO_2 uptake induced by wind forcing: quantification and spatial analysis.
499 *Biogeosciences, 15*(6), 1701–1720. https://doi.org/10.5194/bg-15-1701-2018

500 Sabine, C., Sutton, A., McCabe, K., Lawrence-Slavas, N., Alin, S., Feely, R., et al. (2020).
501 Evaluation of a new carbon dioxide system for autonomous surface vehicles. *Journal of*
502 *Atmospheric and Oceanic Technology, 37*(8), 1305–1317.
503 https://doi.org/10.1175/JTECH-D-20-0010.1

504 Sutton, A. J.; Battisti, R., Maenner Jones, S., Musielewicz, S., Bott, R., Osborne, J. (2020).
505 Surface underway measurements of partial pressure of carbon dioxide (pCO_2), sea
506 surface temperature, sea surface salinity and other parameters from Autonomous Surface
507 Vehicle ASV_Saildrone1020 (EXPOCODE 32DB20190119) in the South Atlantic
508 Ocean, South Pacific Ocean, Indian Ocean and Southern Ocean from 2019-01-19 to
509 2019-08-03 (NCEI Accession 0221912). NOAA National Centers for Environmental
510 Information. doi: https://doi.org/10.25921/6zja-cg56.

511 Sutton, A. J., Sabine, C. L., Maenner-Jones, S., Lawrence-Slavas, N., Meinig, C., Feely, R. A., et
512 al. (2014). A high-frequency atmospheric and seawater pCO_2 data set from 14 open-
513 ocean sites using a moored autonomous system. *Earth System Science Data, 6*(2), 353–
514 366. https://doi.org/10.5194/essd-6-353-2014

515 Sutton, A. J., Wanninkhof, R., Sabine, C. L., Feely, R. A., Cronin, M. F., & Weller, R. A.
516 (2017). Variability and trends in surface seawater pCO_2 and CO_2 flux in the Pacific
517 Ocean. *Geophysical Research Letters, 44*(11), 5627–5636.
518 https://doi.org/10.1002/2017GL073814

519 Takahashi, T., Sutherland, S. C., Wanninkhof, R., Sweeney, C., Feely, R. A., Chipman, D. W., et
520 al. (2009). Climatological mean and decadal change in surface ocean pCO_2, and net sea-
521 air CO_2 flux over the global oceans. *Deep Sea Research Part II: Topical Studies in*
522 *Oceanography, 56*(8-10), 554–577. https://doi.org/10.1016/j.dsr2.2008.12.009

523 Takahashi, T., Sweeney, C., Hales, B., Chipman, D. W., Newberger, T., Goddard, J. G., et al.
524 (2012). The changing carbon cycle in the Southern Ocean. *Oceanography, 25*(3), 26–37.

525 Tomita, H., Kawai, Y., Cronin, M. F., Hihara, T., & Kubota, M. (2015). Validation of AMSR2
526 sea surface wind and temperature over the Kuroshio Extension region. *SOLA, 11*, 43–47.

527 Wallcraft, A. J., Kara, A. B., Barron, C. N., Metzger, E. J., Pauley, R. L., & Bourassa, M. A.
528 (2009). Comparisons of monthly mean 10 m wind speeds from satellites and NWP
529 products over the global ocean. *Journal of Geophysical Research: Atmospheres,*
530 *114*(D16), D16109. https://doi.org/10.1029/2008JD011696

531 Wanninkhof, R. (2014). Relationship between wind speed and gas exchange over the ocean
532 revisited. *Limnology and Oceanography: Methods, 12*(6), 351–362.
533 https://doi.org/10.4319/lom.2014.12.351

534 Watson, A. J., Schuster, U., Shutler, J. D., Holding, T., Ashton, I. G. C., Landschützer, P., et al.
535 (2020). Revised estimates of ocean-atmosphere CO2 flux are consistent with ocean

536   carbon inventory. *Nature Communications*, 11(1), 4422. https://doi.org/10.1038/s41467-
537   020-18203-3

538   Weiss, R. F. (1974). Carbon dioxide in water and seawater: the solubility of a non-ideal gas.
539   *Marine Chemistry, 2*(3), 203–215. https://doi.org/10.1016/0304-4203(74)90015-2

540   Weiss, R. F., Jahnke, R. A., & Keeling, C. D. (1982). Seasonal effects of temperature and
541   salinity on the partial pressure of CO_2 in seawater. *Nature, 300*(5892), 511–513.
542   https://doi.org/10.1038/300511a0

543   Weissman, D. E., Stiles, B. W., Hristova-Veleva, S. M., Long, D. G., Smith, D. K., Hilburn, K.
544   A., & Jones, W. L. (2012). Challenges to satellite sensors of ocean winds: Addressing
545   precipitation effects. *Journal of Atmospheric and Oceanic Technology, 29*(3), 356–374.
546   http://doi.org/10.1175/JTECH-D-11-00054.1

547   Weller, R. A. (2015). Variability and trends in surface meteorology and air–sea fluxes at a site
548   off northern Chile. *Journal of Climate, 28*(8), 3004-3023. https://doi.org/10.1175/JCLI-
549   D-14-00591.1

550   Williams, N. L., Juranek, L. W., Feely, R. A., Johnson, K. S., Sarmiento, J. L., Talley, L. D., et
551   al. (2017). Calculating surface ocean pCO_2 from biogeochemical Argo floats equipped
552   with pH: An uncertainty analysis. *Global Biogeochemical Cycles, 31*(3), 591–604.
553   https://doi.org/10.1002/2016GB005541

554   Zhang, D., Cronin, M. F., Meinig, C., Farrar, J. T., Jenkins, R., Peacock, D., et al. (2019).
555   Comparing air-sea flux measurements from a new unmanned surface vehicle and proven
556   platforms during the SPURS-2 field campaign. *Oceanography, 32*(2), 122–133.
557   https://doi.org/10.5670/oceanog.2019.220